Pulse Compression Favorable Thermal Wave Imaging Techniques for Non-Destructive Testing and Evaluation of Materials

Ravibabu Mulaveesala, Vanita Arora, and Geetika Dua

***Abstract*—This article highlights the application of pulse compression favorable Frequency Modulated Thermal Wave Imaging (FMTWI) technique for testing and evaluation of Carbon Fibre Reinforced Plastics (CFRP). The concept of InfraRed Image Correlation (IRIC) has been introduced to reconstruct the correlation fringes for the pulse compressed data obtained from the matched filter approach to detect the flat bottom hole defects in a CFRP specimen. Further, comparison has been made with the acquired phasegrams using frequency and time domain based data processing approaches. Obtained results clearly demonstrate the strengths of the proposed IRIC based post-processing scheme in providing the spatio-temporal correlation fringes for thermal Non-Destructive Testing & Evaluation (NDT&E) of CFRP materials.**

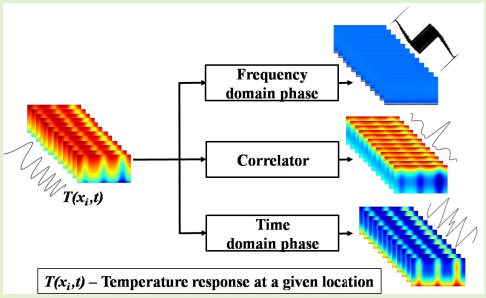

***Index Terms*—Carbon fibre reinforced plastic, correlation fringes, frequency modulated thermal wave imaging, non-destructive testing.**

I. Introduction

CARBON fibre reinforced plastic (CFRP) materials are being increasingly used in modern aerospace, automobile, civil, electrical, electronic and mechanical engineering industries due to their high strength to weight ratio. However, various defects can occur in composites during the manufacturing or in-service phase which reduces their mechanical performance. Therefore, rigorous Non-Destructive Testing & Evaluation (NDT&E) method is demanded to assure the structural integrity of composites.

Manuscript received October 4, 2020; revised October 22, 2020; accepted October 27, 2020. Date of publication October 30, 2020; date of current version May 28, 2021. This work was supported in part by the Science and Engineering Research Board (SERB), Department of Science and Technology, Government of India, under Grant SB/S3/EECE/089/2014, in part by the Global Innovation and Technology Alliance (GITA) from the project entitled "The Development of a Portable THERMOgraphy Based Health DeTECTion System (THERMOTECT) in breast cancer screening" under Grant 2016UK0202022 |IN-UK RFP 2016, and in part by the Aeronautics Research and Development Board (AR&DB), Government of India, under Grant DRDO/08/2031732/M/I on 29. 05. 2014. The associate editor coordinating the review of this article and approving it for publication was Dr. Marko Vauhkonen. *(Corresponding author: Ravibabu Mulaveesala.)*

Ravibabu Mulaveesala is with the Indian Institute of Technology Ropar, Ropar 140001, India (e-mail: ravi@iitrpr.ac.in).

Vanita Arora is with the Indian Institute of Information Technology Una, Una 177220, India.

Geetika Dua is with the Thapar Institute of Engineering and Technology, Patiala 147004, India.

Digital Object Identifier 10.1109/JSEN.2020.3034823

Currently, various NDT&E methods have been employed to identify defects in fibre reinforced composites such as ultrasonic testing, eddy current testing, and radiographic testing. These techniques are well studied in literature and are established for the quality control of composites. Nevertheless, each method has its own advantages and limitations to adopt for inspection of fibre reinforced plastics. Active Thermal Wave Imaging (TWI) techniques are now extensively used for the health monitoring of composite materials used in various industrial applications [1]–[3]. This is because of their inherent testing capabilities (such as full-field, fast and remote inspection). Conventional active optical TWI test procedure involves the application of modulated thermal stimulus onto the test material using optical heat sources such as halogen lamps, LASER etc. This causes a thermal perturbation over the surface of the test specimen and induces thermal waves inside it. As the thermal waves propagate inside the specimen by diffusion, the thermal distribution over a defective area differ from that of the sound causing temperature gradients over the specimen. The resultant thermal response over the specimen is recorded by an infrared camera and is analyzed to evaluate surface and sub-surface anomalies. To improve the signal-to-noise (SNR) ratio for enhanced resolvability of the sub-surface defects, various post-processing methods have to be employed on the captured data [4]–[12].

Depending on the type of external thermal stimulus used to generate thermal waves, widely used optically stimulated thermography methods are classified as Pulse Thermography (PT) [4], [5] and Lock-in Thermography (LT) [6]–[8]. PT is a simple and fast thermographic technique that uses a short-duration high peak power pulse to induce the thermal waves into the specimen. Very short duration pulses (ranging from few milliseconds to a few seconds) are typically employed, depending on the specimen thermal properties and its thickness. The recorded thermal response over the specimen is recorded and is used to reveal the defects inside the test material. The main limitation of this approach is the requirement of high peak power heat sources for the inspection of thick specimen. Also the obtained thermal distribution for PT, is not only influenced by hidden defects but also affected by surface emissivity variations and non-uniform heating. Further, the high peak power heat sources may cause damage to the specimen under test. Whereas, Lock-in thermography (LT) works on the principle of application of periodically modulated heat input onto the test specimen at a certain fixed frequency using considerably low peak power heat sources. Further, unlike PT, LT utilizes the phase images to reveal the information regarding the sub-surface defects. Since phase images are less sensitive to non-uniform heating and surface emissivity variations over the test specimen which helps to detect the deep defects inside the test specimen. Even though LT requires moderate peak power heat sources and the retrieved phase information enables the sub-surface defect detection with higher SNR, as LT uses mono-frequency thermal excitation over the specimen which limits the depth resolution to a fixed value [12]. In order to locate defects located at various depths inside the test specimen, it demands repetition of the test at different frequencies, which makes it a time consuming process. In order overcome the limitations limited resolution of LT and surface emissivity variations as well as non-uniform heating effects of PT, Pulse Phase Thermography (PPT) was introduced [9]–[11]. PPT even though combines the advantages of LT and PT but still the requirement of high peak power heat sources is a limitation to detect the deep defects inside the test sample.

To overcome the above said limitations of the conventional thermographic techniques, the present experimental work focuses on a non-periodic pulse compression favourable thermal excitation technique named as Frequency Modulated Thermal Wave Imaging (FMTWI). This technique makes use of the advantage of non-periodic thermal wave excitation composed of a chosen band of frequencies in a single experimentation cycle based on thermal properties of the test specimen and its thickness [12]. Hence, this method facilitates complete depth scanning, enabling defect detection at different depths in a single run.

Further among various conventional data-processing approaches such as frequency domain phase, thermal signal reconstruction, principal component analysis, recently proposed cross-correlation based time domain analysis scheme utilizes the potential capabilities of energy concentration in time to improve the test resolution and sensitivity even with usage of moderate peak power heat sources in a limited span of experimentation time [13]–[15] in comparison with the conventional pulse and lock-in-thermographic techniques. This article highlights the capabilities of the temporal correlation fringes obtained from the time domain based matched filter based data processing scheme for the detection of sub-surface defects in a CFRP specimen using the infrared image correlation fringes and compares the detection capabilities with conventional phase approaches [16]–[20].

II. Theory

For a given incident heat stimulus, heat diffusion through a solid is not only influenced by material thermal properties but also the anomalies present within it. This leads to temperature gradient over the specimen surface with respective to the sound region. The resultant thermal data for a given frequency modulated thermal stimulus is described by Fourier one-dimensional heat diffusion equation in the absence of any heat source and sink as follows [12]:

$$\frac{\partial^2 T\,(x,t)}{\partial x^2} = \frac{1}{\alpha}\frac{\partial T\,(x,t)}{\partial t} \tag{1}$$

where $T(x,t)$ is the temperature at a given spatial location x and at a given time t and α is the thermal diffusivity of the specimen. The obtained steady-state solution for a linear frequency modulated thermal wave propagating through a semi-infinite solid is expressed as follows [12]:

$$T\,(x,t) = T_0 e^{-x\sqrt{\frac{\pi}{\alpha}\left(f+\frac{Bt}{\tau}\right)}} e^{-jx\sqrt{\frac{\pi}{\alpha}\left(f+\frac{Bt}{\tau}\right)}} e^{2\pi j\left(ft+\frac{Bt^2}{2\tau}\right)} \tag{2}$$

where T_0 is the maximum temperature, f is the initial frequency, B is the bandwidth and τ is the total duration of excitation. Penetrating thermal wave gets attenuated as it propagates through the specimen. The depth at which the energy of wave decays to $1/e$ times of its surface value is called thermal diffusion length and is given by [12]:

$$\mu' = \sqrt{\frac{\alpha}{\pi\left(f+\frac{Bt}{\tau}\right)}} \tag{3}$$

Here B/τ is the frequency sweep rate of a linear frequency modulated signal, which specifies the rate of change of frequency with time. The relation between diffusion length and bandwidth of the applied heat stimulus determines complete depth scanning by employing a suitable frequency range in a single run. If the frequency sweep rate (B/τ) [15] is kept zero, then the diffusion length equation becomes similar to that of the diffusion length for lock-in thermography.

A. An Overview on Active Thermographic Excitation Signals

This section gives a quick overview of basic thermal excitation schemes widely used for active infrared thermography along with the associated signal processing approaches for testing and evaluation of sub-surface defects. Various non-periodic and periodic thermal excitation schemes have been discussed in terms of defect detection sensitivity and resolution. Further, emphasis has been given to correlation based post-processing approach to achieve better sensitivity

and test resolution for detecting the sub-surface defects located at various depths inside the test specimen.

Let a sinusoidal modulated incident heat flux generates a similar temperature distribution over the test specimen with reduction in amplitude, significant time delay and a mean raise in temperature during the heating period. Let's consider the temporal temperature distribution obtained at a given spatial position over the test specimen be $s(t)$ (results due to the exciting incident heat flux) by neglecting the mean raise during the active heating is expressed as [13]–[15]:

$$s\,(t) = a\,(t)\,.\cos[2\pi f_c t + \varphi\,(t)] \tag{4}$$

where t is the time [s], $a(t)$ is the amplitude, f_c is the carrier frequency [Hz] and $\varphi(t)$ is the phase of the sinusoidal function. The argument of sine in equation (4) is the phase function $\Phi(t)$ of the signal and it is given as:

$$\Phi\,(t) = 2\pi f_c t + \varphi(t) \tag{5}$$

If $\varphi(t)$ is a continuous time function, the time derivative of the phase can be expressed as the instantaneous frequency f_i:

$$f_i = \frac{1}{2\pi}\frac{d\Phi(t)}{dt} = f_c + \frac{1}{2\pi}\frac{d\varphi(t)}{dt} \tag{6}$$

From equation (5) it can be seen that the phase modulation function has to be a non-linear function of time, since any linear term can be combined with a carrier frequency. If the amplitude $a(t)$ varies slowly compared to the instantaneous frequency f_i, $|a(t)|$ represents essentially the envelope of the temporal temperature distribution.

The Fourier Transform of the $s(t)$ (Figure 1 (a)) is denoted as $S(f)$ (Figure 1 (b)), f is the frequency [Hz]. $s(t)$ and $S(f)$ are related through the Fourier integrals [13]–[15].

$$\begin{aligned} S(f) &= \int_{-\infty}^{+\infty} s\,(t)\,.e^{-j2\pi f t}dt \\ s\,(t) &= \int_{-\infty}^{+\infty} S\,(f)\,.e^{j2\pi f t}df \end{aligned} \tag{7}$$

The energy (E) [J] of the temporal temperature signal response is given by:

$$E = \int_{-\infty}^{+\infty}[s(t)]^2 dt = \int_{-\infty}^{+\infty}|S\,(f)|^2\,df \tag{8}$$

where the second part of the equation is obtained by Parseval's equation.

Substituting equation (4) in equation (8), we obtain

$$\begin{aligned} E = &\frac{1}{2}\int_{-\infty}^{+\infty}[a\,(t)]^2 dt \\ &+ \frac{1}{2}\int_{-\infty}^{+\infty}[a\,(t)]^2\cos\{2\,[2\pi f_c t + \varphi\,(t)]\}dt \end{aligned} \tag{9}$$

For narrow band signals, in general the frequencies contained in the function $a(t)$ and $\varphi(t)$ are small compared to the carrier frequency f_c. In this case, the second integral represents the oscillation of a sine under a slowly varying envelope and is essentially zero. Then, the energy can be approximated by [13]–[15]:

$$E \approx \frac{1}{2}\int_{-\infty}^{+\infty}[a\,(t)]^2 dt \tag{10}$$

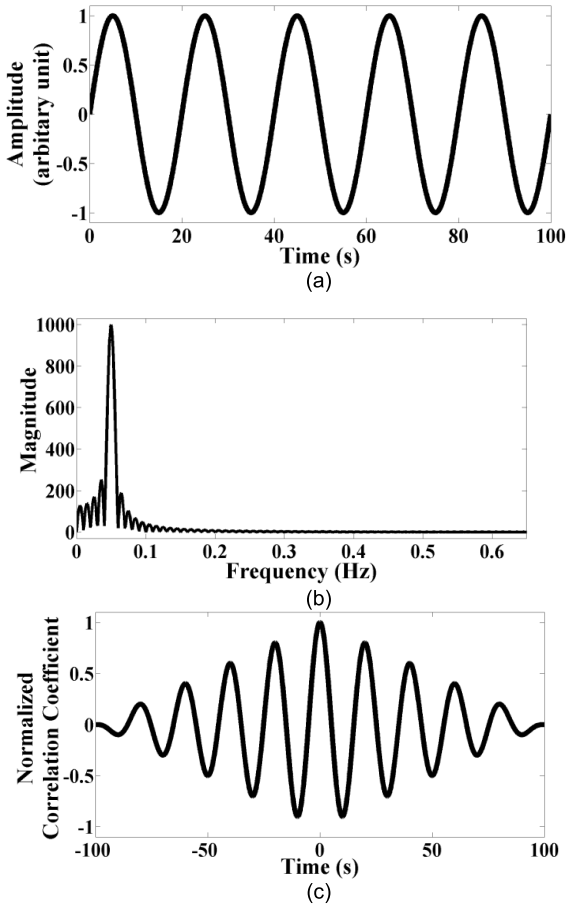

Fig. 1. Schematic of (a) sinusoidal imposed excitation (b) frequency response of the mean removed recorded temporal temperature distribution over the specimen and (c) the auto-correlation profile of the mean zero temporal temperature distribution.

This result shows that as long as the phase modulation does not distort the signal envelope, the signal energy is not altered. The auto-correlation function is defined by the integral:

$$R_{ss}\,(\tau) = \int_{-\infty}^{+\infty} s\,(t)\,s\,(t-\tau)\,dt = \int_{-\infty}^{+\infty}|S\,(f)\,|^2 e^{i2\pi f\tau}df \tag{11}$$

The auto-correlation shows how different a signal is compared to its shifted version as a function of the time shift τ. The maximum occurs when $\tau = 0$ (Figure 1 (c)) and is equal to the signal energy:

$$R_{ss,\max}|_{\tau=0} = \int_{-\infty}^{+\infty}[s\,(t)]^2 dt = E \tag{12}$$

B. Complex Notation of Narrowband Excitation Signals

The excitation and the corresponding temperature responses in active thermography in practice are real; however the complex notation offers advantages particularly in expressing correlation integrals. The matched filter response for the obtained thermal profile is the key factor in this work, computed with a suitable post-processing approach using correlation integrals for the aperiodic thermal wave imaging methods such as frequency modulated thermal wave imaging. Therefore, the use of complex notations is much more convenient.

Since the spectrum of the real signal is symmetric around the zero frequency, an equivalent but simplified notation is a complex signal that has no zero frequencies and double the amplitude of the positive frequencies. A complex signal is called analytic if the spectrum consists of only positive frequencies. This is possible when the real and imaginary parts of the signal form a Hilbert pair. Let

$$\psi(t) = \mu(t).e^{j2\pi f_c t} \tag{13}$$

be an analytic signal, whose real part is equal to the modulated signal in equation (4), $\mu(t)$ is a complex function with magnitude $|\mu(t)|$ and phase $\phi(t)$, usually referred to as the complex envelope, and combines amplitude and phase modulation:

$$\mu(t) = |\mu(t)|.e^{j\phi(t)} \tag{14}$$

The real waveform is derived as the real part of the complex signal:

$$s(t) = Re\{\psi(t)\} = |\mu(t)|.\cos[2\pi f_c t + \phi(t)] \tag{15}$$

If $\Psi(f)$ and $M(f)$ are the Fourier Transform of the analytic signal $\psi(t)$ and the complex envelope $\mu(t)$ respectively, the Fourier Transform (FT) of equation (13) yields

$$M(f) = \Psi(f + f_c) \tag{16}$$

Thus, the frequency spectrum of the complex envelope is the shifted spectrum of the signal with a carrier frequency removed. When the real signal is narrow band, the conditions:

$$a(t) \approx |\mu(t)|, \varphi(t) \approx \phi(t) \tag{17}$$

are satisfied and the analytic complex signal is derived from the real signal simply by substituting the cosine with an exponent. Note that the resultant signal (sometimes referred to as *exponential* signal) will not be strictly analytic, if the fractional bandwidth of the real signal is so high, that the spectrum of the exponential signal falls over the negative frequencies.

Using the second part of equation (8) and the fact that $\Psi(f) = 2S(f)$ for positive frequencies, the energy can now be written as [13]–[15]:

$$\begin{aligned} E &= \int_{-\infty}^{+\infty} |S(f)|^2 df = \int_0^{\infty} \left|\frac{1}{2}\Psi(f)\right|^2 df \\ &= \frac{1}{2}\int_{-\infty}^{\infty} |\Psi(f)|^2 df \\ &= \frac{1}{2}\int_{-\infty}^{\infty} [\psi(t)]^2 dt = \frac{1}{2}\int_{-\infty}^{\infty} |\mu(t)|^2 dt \\ &= \frac{1}{2}\int_{-\infty}^{\infty} |M(f)|^2 df \end{aligned} \tag{18}$$

The equality sign in the later part of equation (18) is exact, as opposite to the approximation in equation (10). This is another indication that going from real to the complex notation is only an approximation. In the rest of the analysis, it is assumed that the exponential signal is a good approximation of the analytic signal, an assumption that it is reasonable for the relatively narrow band signals that can excite the heat source.

C. Correlation Integrals

In a similar manner to the definition given in equation (11), the complex auto-correlation of $\psi(t)$ is given by:

$$\begin{aligned} R_{\psi\psi}(\tau) &= \int_{-\infty}^{+\infty} \psi(t)\psi^*(t-\tau)\, dt \\ &= \int_{-\infty}^{+\infty} |\Psi(f)|^2 e^{j2\pi f\tau} df \end{aligned} \tag{19}$$

Using equation (13) and equation (16), the auto-correlation function can be expressed as a function of modulation [13]–[15]:

$$\begin{aligned} R_{\psi\psi}(\tau) &= e^{j2\pi f_c\tau} \int_{-\infty}^{+\infty} \mu(t)\mu^*(t-\tau)\, dt \\ &= e^{j2\pi f_c\tau} \int_{-\infty}^{+\infty} |M(f)|^2 e^{j2\pi f\tau} df \end{aligned} \tag{20}$$

In an imaging system, the displayed quantity is the envelope of the signal. The envelope of the real auto-correlation function is the matched-filter response, and it is in fact the inverse Fourier transform of the modulation's energy density spectrum $|M(f)|^2$:

$$\begin{aligned} Env\{R_{ss}(\tau)\} &= \frac{1}{2}\left|R_{\psi\psi}(\tau)\right| = \frac{1}{2}\left|\int_{-\infty}^{+\infty} \mu(t)\mu^*(t-\tau)\, dt\right| \\ &= \frac{1}{2}\left|\int_{-\infty}^{+\infty} |M(f)|^2 e^{j2\pi f\tau} df\right| \end{aligned} \tag{21}$$

Figure 2 sketches the application of equation (21) in the estimate of the auto-correlation envelope of a single-carrier pulse of duration T (Figure 2 (a)). In the absence of modulation, $\mu(t)$ is a real-valued rectangular window. The modulus of its FT $M(f)$ is a sinc function (Figure 2 (b)), and the inverse FT of a sinc^2 function is the triangle function (Figure 2 (c)).

D. Applicability of Correlation Integrals for Some of the Widely Used Excitation Signals in Active Thermography

This section deals with the applications of correlation integrals for widely used transient and steady-state active thermographic methods. The most popular active infrared thermographic techniques are pulse thermography [4], [5], lock-in thermography [6]–[8], pulse phase thermography [9]–[11] and frequency modulated thermal wave imaging [18]–[29]. Among these methods, except PT, the adopted popular post-processing approach is the frequency domain phase extraction in order to detect sub-surface defects in the test specimen. The results obtained from this approach are insensitive to surface emissivity variations and non-uniform heating over the specimen in addition to its deeper depth of penetration.

In general, phasegrams are reconstructed by applying the FT onto the captured thermograms during the experimentation. These phasegrams obtained at a particular frequency are used for detection of sub-surface defects. Due to the adopted frequency domain reconstruction process, the total supplied energy is redistributed to the individual frequency components. This disintegration of the supplied energy to individual frequency components under consideration, limits the applicability of the frequency domain data analysis schemes. In addition to this, phasegram obtained at a particular

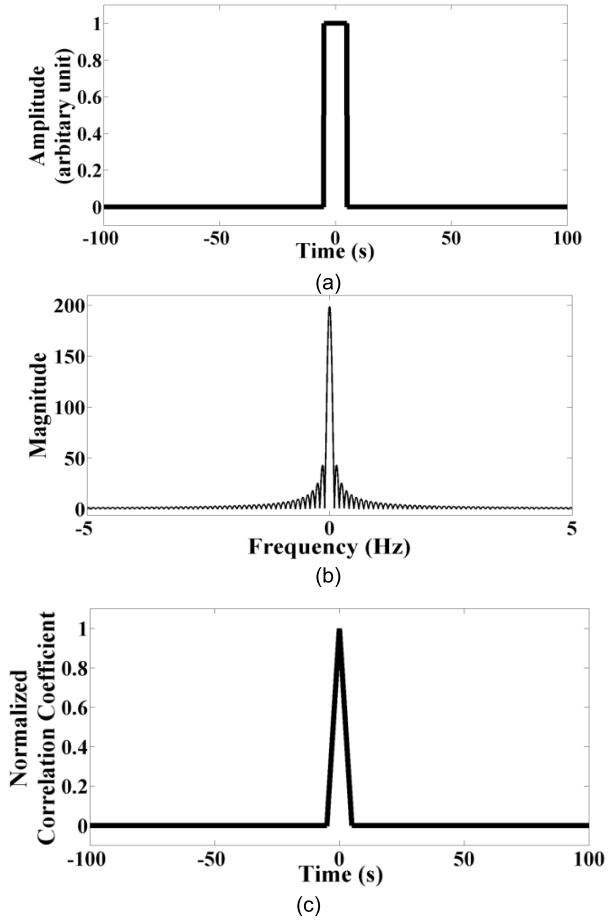

Fig. 2. Schematic of (a) pulse shaped imposed excitation (b) frequency response of the captured temporal temperature distribution recorded over the specimen and (c) the auto-correlation profile of the temporal temperature distribution.

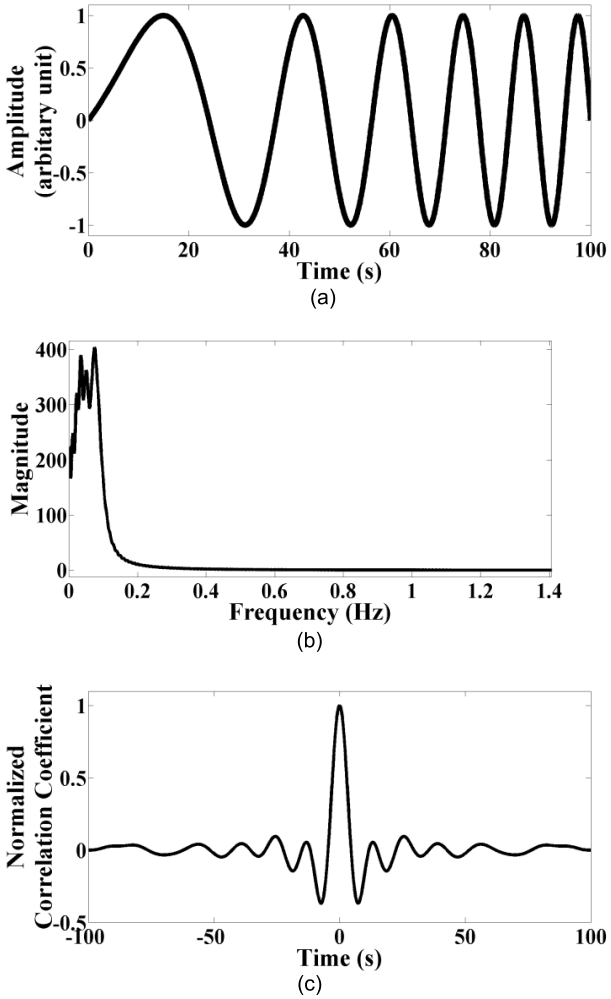

Fig. 3. Schematic of (a) frequency modulated imposed thermal excitation (b) frequency response of the mean removed captured temporal temperature distribution over the specimen and (c) the auto-correlation profile of the mean zero temporal temperature distribution.

frequency limits the test resolution due to its fixed probing wavelength. These limitations can be overcome by considering the time-domain data processing schemes.

Among the most widely used time-domain data processing schemes, this work concentrates mainly on matched filter based analysis. It is clear that the widely used thermal excitation schemes such as lock-in thermography (sinusoidal (Figure 1 (a)) and pulsed (pulse and pulse phase thermography) thermographic techniques (Figure 2 (a)) do not provide the energy concentration (compressed pulses) after correlating the temporal temperatures responses captured over the test specimen with respect to a chosen reference temporal thermal response (Figure 1 (c) and Figure 2 (c)). So the correlation approach currently adopted to these conventional thermographic techniques is not really superior. The presented work mainly concentrates on pulse compression favorable thermal excitation schemes rather than conventional thermal approaches.

The matched filter approach [13]–[15] adopted in the present work is correlation based post-processing data analysis scheme. Due to its merits, such as, results obtained from this approach are immune to random noises generated during the experimentation such as multiplicative noises (non-uniform illumination, emissivity variations over the specimen surface) as well as the additive noise generated in the detection process.

Figure 3 (a) shows the linear frequency modulated thermal excitation used to drive the heat sources in pulse compression favourable active thermography (with frequency varying from 0.01 Hz-0.1 Hz (Figure 3 (b)) for a duration of 100 s) and its corresponding normalized auto-correlation (pulse compressed) thermal response. It's clear from Figure 3 (c) that the obtained auto-correlation function concentrates the supplied energy into a narrow duration high peak power pulse which improves the test sensitivity and resolution. This approach is more prevalent in radar, sonar to enhance the range resolution with improved sensitivity even in a noisy environment. It allows the imposed heat flux using moderate peak power heat sources and produces the resolution and sensitivity similar to the results obtained with narrow duration high peak power impulse excitation.

The following two data-processing schemes are employed on the temporal thermal response obtained from equation 2 at a given spatial location.

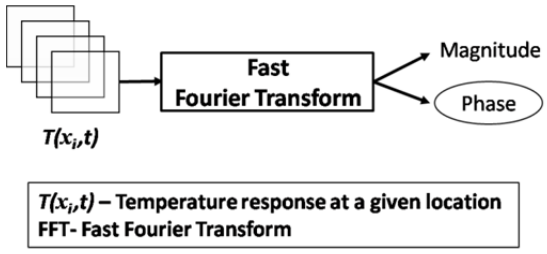

Fig. 4. Data processing to obtain frequency domain based phasegrams.

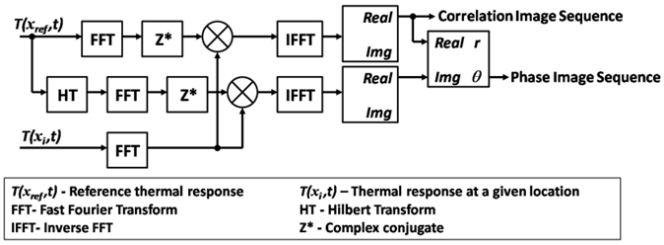

Fig. 5. Data processing to obtain time domain based phasegrams and correlation coefficient images.

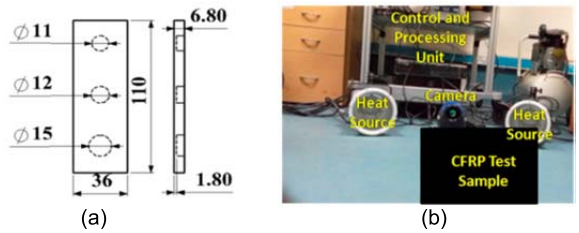

(a) (b)

Fig. 6. (a) top and cross-sectional views of the experimental CFRP specimen (all dimensions are in mm), (b) shows the experimental set up.

1) Frequency Domain Based Analysis Scheme [9], [10]: In this approach, 1-dimensional Fast Fourier Transform (FFT) is carried out on the captured temporal temperature response of each pixel $T(x_i,t)$ (where x_i is the index in the thermal image sequence) in the field of view as mentioned below:

$$F(u) = \frac{1}{N}\sum_{n=0}^{N-1} T(x_n,t)e^{\left[\frac{-j2\pi u x_n}{N}\right]} = R(u) + jI(u) \quad (22)$$

where $R(u)$ and $I(u)$ are the real and imaginary components of $F(u)$ respectively. The phasegrams are then reconstructed by using the real and imaginary components as follows:

$$\emptyset(u) = tan^{-1}\left(\frac{I(u)}{R(u)}\right) \quad (23)$$

2) Time Domain Based Analysis Scheme [18]–[24]: In this approach, Hilbert Transform (HT) is used to extract correlation coefficient and time domain based phasegrams from the captured temporal temperature distribution as follows:

$$H(t) = \frac{1}{\pi}\int_{-\infty}^{\infty}\frac{T(x_r,\tau)}{t-\tau}d\tau \quad (24)$$

where $T(x_r,t)$ is chosen sound (non-defective region) reference thermal signal. The cross-correlation coefficient is computed

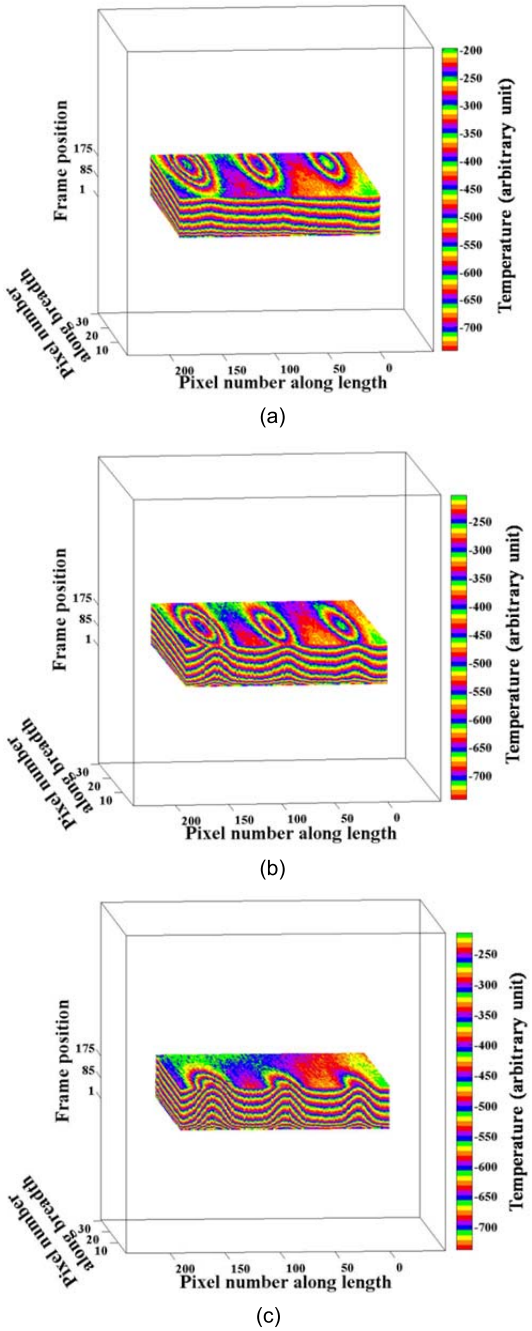

Fig. 7. Mean-removed image sequence. (a)–(c) show the stack of mean-removed thermal images obtained for a duration of 8.75 s for three different cross-sectional slices.

by using Inverse Fast Fourier Transform (IFFT) given as:

$$Correlation\ coefficient = IFFT\left\{T(x_r,\omega)^* T(x_i,\omega)\right\} \quad (25)$$

where $T(x_r,\ \omega)$ and $T(x_i,\ \omega)$ are the Fourier transforms of the chosen (non-defective region) reference response and temporal thermal response at a given location respectively. The time domain phase of the thermal wave signal is then reconstructed as:

$$\theta = tan^{-1}\left(\frac{IFFT\left\{H(\omega)^* T(x_i,\omega)\right\}}{IFFT\left\{T(x_r,\omega)^* T(x_i,\omega)\right\}}\right) \quad (26)$$

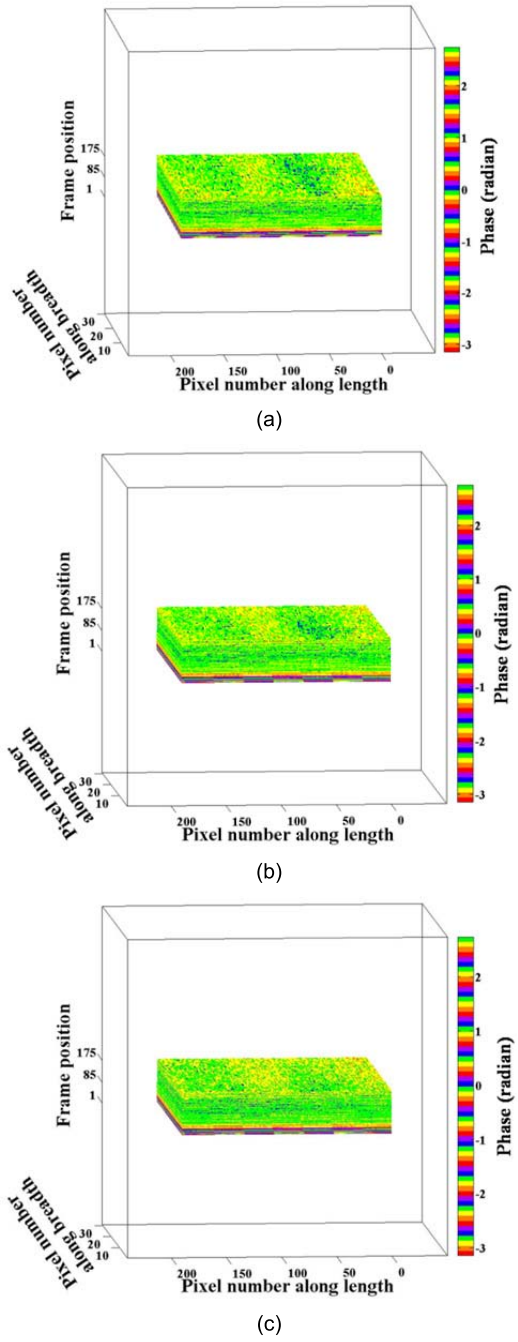

Fig. 8. Frequency domain based phasegrams. (a)–(c) illustrate the stack of frequency domain phasegrams within the frequency range of 0.01-0.018 Hz for three different cross-sectional slices.

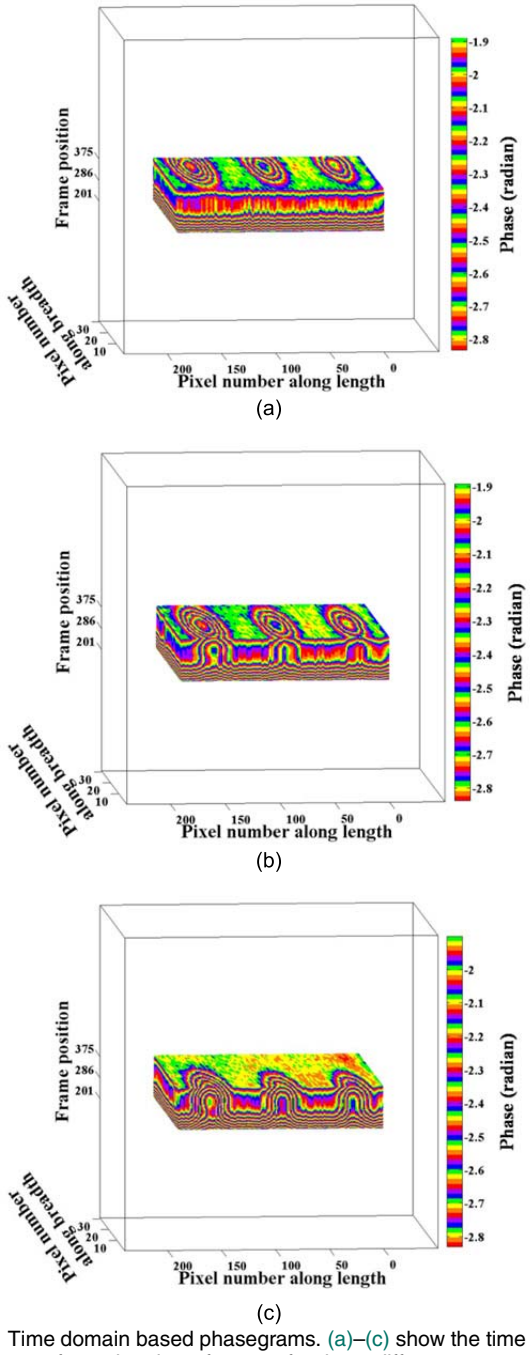

Fig. 9. Time domain based phasegrams. (a)–(c) show the time domain phasegrams for a duration of 8.75 s for three different cross-sectional slices.

III. Test Specimen and Experimentation

To test the defect detection capabilities of the proposed technique, a CFRP specimen of size 36×110 mm is taken into consideration. The specimen contains three circular shaped flat bottom hole defects of 5.50, 6 and 7.5 mm radii kept at a depth of 1.8 mm from the front surface of the specimen having 6.8 mm thickness, as shown in Figure 6 (a).

A linear chirp heat stimulus with frequencies varying from 0.01 Hz to 0.1 Hz for 100 s duration, is imposed onto the specimen with the help of two heat sources delivering a power of 500 W each as shown in Figure 6 (b). The resultant temporal temperature response is captured at a capturing frequency of 20 Hz for duration of 100 s using a FLIR SC 5500 high-speed, science grade 14-bit infrared camera, which has a 320 × 256 resolution.

The mean raise in the recorded thermal data during the active heating is removed using a suitable polynomial fit. To enhance the defect signature, frequency and time domain based data-processing schemes are employed on the mean-removed thermal data.

IV. Results and Discussion

Figure 7 (a)-(c) show the stack of mean-removed thermal images obtained for a duration of 8.75 s for three

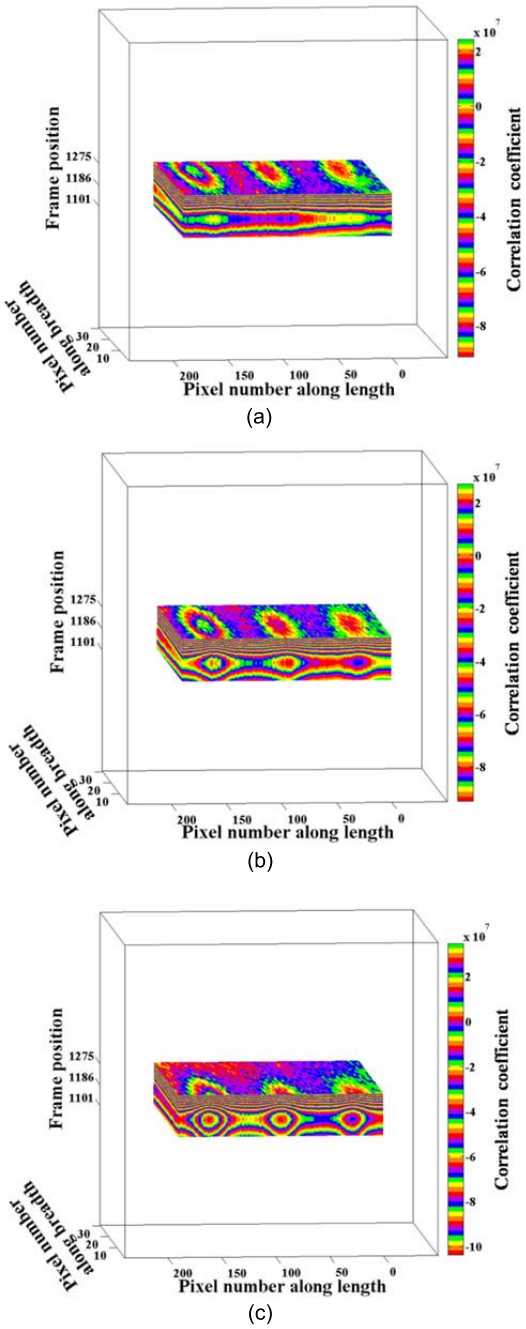

Fig. 10. Correlation coefficient image sequence. (a)–(c) show the correlation coefficient images for a duration of 8.75 s for three different cross-sectional slices.

different cross-sectional slices whereas Figure 8 (a)-(c) illustrate the stack of frequency domain phasegrams within the frequency range of 0.01-0.018 Hz for three different cross-sectional slices.

Figure 9 (a)-(c) show the time domain phasegrams for a duration of 8.75 s for three different cross-sectional slices. The correlation coefficient images for a duration of 8.75 s for three different cross-sectional slices are depicted in Figure 10 (a)-(c). The obtained spatio-temporal correlation fringes from the pulse compressed reconstructed temporal thermal sequence clearly illustrates the effect of the depth of defects and its dependency on the number of fringes.

V. Conclusion

In this article, a linear Frequency Modulated Thermal Wave Imaging (FMTWI) technique is experimentally demonstrated on a CFRP specimen containing flat bottom circular shaped holes defects. This technique has shown its potential complementary nature to that of the conventional pulsed and lock-in thermographic NDT techniques as it can scan the entire specimen in a single experimentation cycle using relatively low peak power heat sources. The introduction of pulse compression based spatio-temporal data-processing scheme helps in providing infrared image correlation fringes to visualize the hidden defects in the CFRP test specimen. Experimental results presented in this article demonstrate an unprecedented degree of defect detectability using infrared image correlation fringe based analysis and the results compared the results with conventional phase based approaches.

References

[1] X. P. V. Maldague, *Theory and Practice of Infrared Thermography for Non-Destructive Testing*. Hoboken, NJ, USA: Wiley, 2001.
[2] V. P. Vavilov, "Thermal nondestructive testing of materials and products: A review," *Russian J. Nondestruct. Test.*, vol. 53, no. 10, pp. 707–730, Oct. 2017.
[3] U. Netzelmann, G. Walle, S. Lugin, A. Ehlen, S. Bessert, and B. Valeske, "Induction thermography: Principle, applications and first steps towards standardization," *Quant. Infr. Thermography J.*, vol. 13, no. 2, pp. 170–181, 2016.
[4] D. L. Balageas, J. C. Krapez, and P. Cielo, "Pulsed photothermal modeling of layered materials," *J. Appl. Phys.*, vol. 59, no. 2, pp. 348–357, Jan. 1986.
[5] A. C. Tam, "Pulsed photothermal radiometry for noncontact spectroscopy, material testing and inspection measurements," *Infr. Phys.*, vol. 25, nos. 1–2, pp. 305–313, Feb. 1985.
[6] G. Busse, D. Wu, and W. Karpen, "Thermal wave imaging with phase sensitive modulated thermography," *J. Appl. Phys.*, vol. 71, no. 8, pp. 3962–3965, Apr. 1992.
[7] C. Meola, "Nondestructive evaluation of materials with rear heating lock-in thermography," *IEEE Sensors J.*, vol. 7, no. 10, pp. 1388–1389, Oct. 2007.
[8] W. Bai and B. S. Wong, "Evaluation of defects in composite plates under convective environments using lock-in thermography," *Meas. Sci. Technol.*, vol. 12, no. 2, pp. 142–150, Feb. 2001.
[9] X. Maldague and S. Marinetti, "Pulse phase infrared thermography," *J. Appl. Phys.*, vol. 79, no. 5, pp. 2694–2698, Mar. 1996.
[10] X. Maldague, F. Galmiche, and A. Ziadi, "Advances in pulsed phase thermography," *Infr. Phys. Technol.*, vol. 43, nos. 3–5, pp. 175–181, Jun. 2002.
[11] V. P. Vavilov and S. Marinetti, "Pulse phase thermography and thermal tomography using Fourier transformation," *Russ. J. Nondestruct. Test.*, vol. 35, no. 2, pp. 58–72, 1999.
[12] R. Mulaveesala and S. Tuli, "Theory of frequency modulated thermal wave imaging for nondestructive subsurface defect detection," *Appl. Phys. Lett.*, vol. 89, no. 19, Nov. 2006, Art. no. 191913.
[13] G. Turin, "An introduction to matched filters," *IEEE Trans. Inf. Theory*, vol. IT-6, no. 3, pp. 311–329, Jun. 1960.
[14] G. F. Kirkbright and R. M. Miller, "Cross-correlation techniques for signal recovery in thermal wave imaging," *Anal. Chem.*, vol. 55, no. 3, pp. 502–506, Mar. 1983.
[15] M. Oelze, "Bandwidth and resolution enhancement through pulse compression," *IEEE Trans. Ultrason., Ferroelectr., Freq. Control*, vol. 54, no. 4, pp. 768–781, Apr. 2007.
[16] S. Tuli and R. Mulaveesala, "Defect detection by pulse compression in frequency modulated thermal wave imaging," *Quant. Infr. Thermography J.*, vol. 2, no. 1, pp. 41–54, Jun. 2005.
[17] R. Mulaveesala and S. V. Ghali, "Coded excitation for infrared nondestructive testing of carbon fiber reinforced plastics," *Rev. Sci. Instrum.*, vol. 82, no. 5, May 2011, Art. no. 054902.
[18] R. Mulaveesala, J. S. Vaddi, and P. Singh, "Pulse compression approach to infrared nondestructive characterization," *Rev. Scientific Instrum.*, vol. 79, no. 9, 2008, Art. no. 094901.

[19] N. Tabatabaei, A. Mandelis, and B. T. Amaechi, "Thermophotonic radar imaging: An emissivity-normalized modality with advantages over phase lock-in thermography," *Appl. Phys. Lett.*, vol. 98, no. 16, pp. 163706-1–163706-3, Apr. 2011.
[20] R. Mulaveesala and V. S. Ghali, "Cross-correlation-based approach for thermal non-destructive characterisation of carbon fibre reinforced plastics," *Insight-Non-Destructive Test. Condition Monitor.*, vol. 53, no. 1, pp. 34–36, Jan. 2011.
[21] R. Yang and Y. He, "Optically and non-optically excited thermography for composites: A review," *Infr. Phys. Technol.*, vol. 75, pp. 26–50, Mar. 2016.
[22] S. Laureti *et al.*, "The use of pulse-compression thermography for detecting defects in paintings," *NDT E Int.*, vol. 98, pp. 147–154, Sep. 2018.
[23] P. Tavakolian and A. Mandelis, "Perspective: Principles and specifications of photothermal imaging methodologies and their applications to non-invasive biomedical and non-destructive materials imaging," *J. Appl. Phys.*, vol. 124, no. 16, pp. 1–12, 2018.
[24] G. Silipigni *et al.*, "Optimization of the pulse-compression technique applied to the infrared thermography nondestructive evaluation," *NDT E Int.*, vol. 87, pp. 100–110, Apr. 2017.
[25] S. Laureti, G. Silipigni, L. Senni, R. Tomasello, P. Burrascano, and M. Ricci, "Comparative study between linear and non-linear frequency-modulated pulse-compression thermography," *Appl. Opt.*, vol. 57, no. 18, p. D32, 2018.
[26] S. Wu *et al.*, "Halogen optical referred pulse-compression thermography for defect detection of CFRP," *Infr. Phys. Technol.*, vol. 102, Nov. 2019, Art. no. 103006.
[27] P. Tavakolian, S. Sfarra, G. Gargiulo, K. Sivagurunathan, and A. Mandelis, "Photothermal coherence tomography for 3-D visualization and structural non-destructive imaging of a wood inlay," *Infr. Phys. Technol.*, vol. 91, pp. 206–213, Jun. 2018.
[28] N. Tabatabaei and A. Mandelis, "Thermal coherence tomography using match filter binary phase coded diffusion waves," *Phys. Rev. Lett.*, vol. 107, no. 16, Oct. 2011, 165901.
[29] S. Kaiplavil and A. Mandelis, "Truncated-correlation photothermal coherence tomography for deep subsurface analysis," *Nature Photon.*, vol. 8, no. 8, pp. 635–642, Aug. 2014.

Ravibabu Mulaveesala received the Ph.D. degree from the Indian Institute of Technology Delhi (IIT Delhi), India. He is currently the Head of the Department of Electrical Engineering, Indian Institute of Technology Ropar, India. His research interests include thermal, acoustical, and optical methods for non-invasive/non-destructive imaging technologies. He serves on the editorial or advisory boards for the several refereed journals of the Institute of Physics, the IEEE, the Institution of Engineering and Technology, and Elsevier.

Vanita Arora received the Ph.D. degree from the Indian Institute of Technology Ropar (IIT Ropar), India. She is working as a Faculty Member with the Indian Institute of Information Technology Una, Una, India. Her research interests include the development of infrared imaging technologies for non-invasive/non-destructive testing applications. She serves as a guest editor for several refereed journals.

Geetika Dua received the Ph.D. degree from the Indian Institute of Technology Ropar (IIT Ropar), India. She is working as a Faculty Member with the Thapar Institute of Engineering and Technology, Patiala, India. She serves as a guest editor for several refereed journals. Her research interests include the development of signal, image, and video processing methods for nondestructive testing/noninvasive imaging modalities for inspection of various industrial and biomedical materials.